Photoanisotropic polarization gratings beyond the small recording angle regime

Man Xu[1,3]*, Dick K. G. de Boer[2], Chris M. van Heesch[2], Arthur J. H. Wachters[1] and H. Paul Urbach[1]

[1] *Optics Research Group, Delft University of Technology, Lorentzweg 1, 2628 CJ Delft, The Netherlands*
[2] *Philips Research Laboratory, High Tech Campus 4, 5656 AE Eindhoven, The Netherlands*
[3] *Department of Physics, Imperial College London, Prince Consort Rd. London SW7 2BW, U.K.*
m.xu@imperial.ac.uk

Abstract: Polarization gratings can be realized by polarization holographic recording in photoanisotropic materials. In this paper, we study two types of polarization gratings. One is recorded with two orthogonally circularly (OC) polarized beams and the other one with two orthogonally linearly (OL) polarized beams. The interference of both cases is explored beyond the small recording angle regime. A novel method is proposed to represent the polarization states of the modulation. The diffraction by polarization gratings is studied with rigorous diffraction theory. Simulations based on the Finite Element Method are performed for both OC and OL polarization gratings at small and large recording angles.

OCIS codes: (050.1950) Diffraction gratings; (160.5335) Photosensitive materials; (090.0090) Holography.

References and links

1. J. A. Delaire and K. Nakatani, "Linear and Nonlinear Optical Properties of Photochromic Molecules and Materials," Chem. Rev. **100**, 1817–1846 (2000).
2. L. Nikolova, T. Todorov, M. Ivanov, F. Andruzzi, S. Hvilsted, and P. S. Ramanujam, "Polarization holographic gratings in side-chain azobenzene polyesters with linear and circular photoanisotropy," Appl. Opt. **35**, 3835–3840 (1996).
3. I. Naydenova, L. Nikolova, T. Todorov, F. Andruzzi, S. Hvilsted, and P. S. Ramanujam, "Polarimetric investigation of materials with both linear and circular anisotropy," J. Mod. Opt. **44**, 1643–1650 (1997).
4. S. Sajti, Á. Kerekes, P. Ramanujam, and E. Lőrincz, "Response function for the characterization of photo-induced anisotropy in azobenzene containing polymers," Appl. Phys. B **75**, 677–685 (2002).
5. M. Schadt, H. Seiberle, and A. Schuster, "Optical patterning of multi-domain liquid-crystal displays with wide viewing angles," Nature **381**, 212–215 (1996).
6. J. N. Eakin, Y. Xie, R. A. Pelcovits, M. D. Radcliffe, and G. P. Crawford, "Zero voltage Freedericksz transition in periodically aligned liquid crystals," Appl. Phys. Lett. **85**, 1671 (2004).
7. M. J. Escuti and W. M. Jones, "Polarization-Independent Switching With High Contrast from a Liquid Crystal Polarization Grating," SID Symp. Dig. **37**, 1443–1446 (2006).
8. C. Provenzano, P. Pagliusi, and G. Cipparrone, "Highly efficient liquid crystal based diffraction grating induced by polarization holograms at the aligning surfaces," Appl. Phys. Lett. **89**, 121105 (2006).
9. H. Sarkissian, B. Park, N. Tabirian, and B. Zeldovich, "Periodically Aligned Liquid Crystal: Potential Application for Projection Displays," Mol. Cryst. Liq. Cryst. **451**, 1–19 (2006).
10. N. Koumura, E. M. Geertsema, A. Meetsma, and B. L. Feringa, "Light-Driven Molecular Rotor: Unidirectional Rotation Controlled by a Single Stereogenic Cente," J. Am. Chem. Soc. **122**, 12,005–12,006 (2000).
11. S. J. Zilker, T. Bieringer, D. Haarer, R. S. Stein, J. W. van Egmond, and S. G. Kostromine, "Holographic Data Storage in Amorphous Polymers," Adv. Mater. **10**, 855 (1998).

#119008 - $15.00 USD Received 29 Oct 2009; revised 19 Dec 2009; accepted 22 Dec 2009; published 17 Mar 2010

12. J. Eickmans, T. Bieringer, S. Kostromine, H. Berneth, and R. Thoma, "Photoaddressable Polymers: A New Class of Materials for Optical Data Storage and Holographic Memories," Jpn. J. Appl. Phys. **38**, 1835–1836 (1999).
13. A. S. Matharu, S. Jeeva, and P. Ramanujam, "Liquid crystals for holographic optical data storage," Chem. Soc. Rev. **36**, 1868–1880 (2007).
14. S. Hvilsted, F. Andruzzi, and P. S. Ramanujam, "Side-chain liquid-crystalline polyesters for optical information storage," Opt. Lett. **17**, 1234–1236 (1992).
15. E. Loerincz, G. Szarvas, P. Koppa, F. Ujhelyi, G. Erdei, A. Sueto, P. Varhegyi, S. Sajti, A. Kerekes, T. Ujvari, and P. S. Ramanujam, "Polarization holographic data storage using azobenzene polyster as storage material," Proc. SPIE **4991**, 34 (2003).
16. L. L. Nedelchev, A. S. Matharu, S. Hvilsted, and P. S. Ramanujam, "Photoinduced Anisotropy in a Family of Amorphous Azobenzene Polyesters for Optical Storage," Appl. Opt. **42**, 5918–5927 (2003).
17. S. D. Kakichashvili, "Regularity in photoanisotropic phenomena," Opt. Spektrosk **52**, 317–322 (1982).
18. S. D. Kakichashvili, "Polarization-holographic recording in the general case of a reaction of a photoanisotropic medium," Kvantovaya Elektron. (Moscow) **10**, 1976–1981 (1983).
19. T. Todorov, L. Nikolova, and N. Tomova, "Polarization holography. 1: A new high-efficiency organic material with reversible photoinduced birefringence," Appl. Opt. **23**, 4309 (1984).
20. T. Todorov, L. Nikolova, and N. Tomova, "Polarization holography. 2: Polarization holographic gratings in photoanisotropic materials with and without intrinsic birefringence," Appl. Opt. **23**, 4588 (1984).
21. T. Todorov, L. Nikolova, K. Stoyanova, and N. Tomova, "Polarization holography. 3: Some applications of polarization holographic recording," Appl. Opt. **24**, 785 (1985).
22. L. Nikolova and T. Todorov, "Diffraction Efficiency and Selectivity of Polarization Holographic Recording," J. Mod. Opt. **31**, 579–588 (1984).
23. L. Nikolova, T. Todorov, M. Ivanov, F. Andruzzi, S. Hvilsted, and P. S. Ramanujam, "Photoinduced circular anisotropy in side-chain azobenzene polyesters," Opt. Mater. **8**, 255–258 (1997).
24. T. Huang and K. H. Wagner, "Holographic diffraction in photoanisotropic organic materials," J. Opt. Soc. Am. A **10**, 306 (1993).
25. T. Huang and K. H. Wagner, "Coupled Mode Analysis of Polarization Volume Hologram," IEEE J. Quantum Electron. **31**, 372 (1995).
26. C. Oh and M. J. Escuti, "Time-domain analysis of periodic anisotropic media at oblique incidence: an efficient FDTD implementation," Opt. Express **14**, 11,870–11,884 (2006).
27. C. M. van Heesch, "Polarization-Selective Diffraction for Display applications," Ph.D. thesis, Eindhoven University of Technology, Eindhoven (2007).
28. B. Kilosanidze and G. Kakauridze, "Polarization-holographic gratings for analysis of light. 1. Analysis of completely polarized light," Appl. Opt. **46**, 1040–1049 (2007).
29. M. Xu, "Diffractive Optics of Anisotropic Polarization Gratings," Ph.D. thesis, Delft University of Technology, Delft (2009).
30. M. Attia and J. M. C. Jonathan, "Anisotropic Gratings Recorded from Two Circular Polarized Coherent Waves," Opt. Commun. **47**, 85–90 (1983).
31. M. Born and E. Wolf, *Principles of Optics*, 7th ed. (Cambridge University Press, 1999).
32. X. Wei, "Three Dimensional Rigorous Model for Optical Scattering Problems," Ph.D. thesis, Delft University of Technology, Delft (2006).
33. X. Wei, A. J. Wachters, and H. P. Urbach, "Finite-element model for three-dimensional optical scattering problems," J. Opt. Soc. Am. A **24**, 866–881 (2007).
34. "ILUPACK V2.1," URL `http://www.math.tu-berlin.de/ilupack/`.
35. O. Schenk and K. Gärtner, "Solving Unsymmetric Sparse Systems of Linear Equations with PARDISO," Journal of Future Generation Computer Systems **20**, 475–487 (2004).
36. O. Schenk and K. Gärtner, "On fast factorization pivoting methods for symmetric indefinite systems," Elec. Trans. Numer. Anal. **23**, 158–179 (2006).

1. Introduction

Photoanisotropic polarization gratings are interesting optical components for many light controlling applications. Such applications include flat panel displays, polarimetry, optical fiber communications, quantum computing, microscopy etc.. Polarization gratings can be manufactured with polarization holographic recording. Depending on the polarization states of the two recording beams and the recording angle, periodic modulation of the polarization states or/and intensity can be achieved. Materials which are sensitive to polarization can be used to record the interference patterns formed by the two beams. A typical material with linear photoanisotropic character, which have been experimentally demonstrated, is azo-dye-doped polymer [1–4]. Chi-

#119008 - $15.00 USD Received 29 Oct 2009; revised 19 Dec 2009; accepted 22 Dec 2009; published 17 Mar 2010

ral dopants are already well known circular birefringent materials. An alternative recording material is the combination of a liquid crystal (LC) and a photo-alignment film (such as, linear-photo-polymers or LPP) [5–9]. Circular birefringence can be obtained by mixing light-driven rotor [10] materials into LCs. In the late 90's, azo polymers have been studied as recording media for both non-binary digital optical storage and holographic storage [11, 12]. Many studies [13–16] on polarization holographic optical data storage have been carried out until nowadays.

Much theoretical work has been done on the recording and the reading process of photoanisotropic polarization gratings. Kakichashvili [17, 18] started research in the field and has built the basic scheme for obtaining the dielectric permittivity changes due to photo-induced anisotropy. Todorov and Nikolova [2, 19–23] have carried out extensive theoretical and experimental work on the recording and reading processes of polarization gratings. They use the Jones Matrix method to study the diffraction from polarization gratings. Coupled mode analysis has been applied to study polarization grating by Huang and Wagner [24, 25]. Oh and Escuti have applied the finite-difference time-domain method (FDTD) to characterize the diffraction of photoanisotropic polarization gratings [26]. Interference of two arbitrary polarizations have been studied by Van Heesch for small recording angles [27]. Recently Kilosanidze has summarized formulations for the recording of linear and circular photoanisotropy [28]. Many other publications which are not listed here contain similar theoretical treatments as those mentioned above. However, in all those papers only paraxial situations are studied, i.e. the recording angle of the two recording beams is small. In [29] we developed a general framework of how to deal with large recording angles in polarization gratings.

As has been observed previously [24, 29], when the recording angles are large, the interference pattern of two plane waves becomes complicated. The plane of polarization varies over one modulation period in 3D space and the approximation that the electric field of the two recording beams are in the same plane does not hold any more [30]. Furthermore, in the small recording angle regime, all polarization states of the interference between two orthogonally polarized beams can be represented in the Poincaré sphere [27]. In contrast, when the recording angle is large the Poincaré Sphere is not sufficient to represent the modulation of the polarization states of the interference. In this paper we will therefore present a novel method to represent the polarization modulation.

Though much research has been done on the diffraction by photoanisotropic polarization gratings, the polarization gratings recorded at large recording angles have not been covered. The main task of this paper is to apply our in-house numerical code based on the finite element method (FEM) to study the diffraction of the photoanisotropic polarization gratings rigorously beyond the small recording angle regime. A brief description of the code is given in Section 3 together with the results and discussions.

2. The polarization states of the interference pattern of two plane waves

2.1. Interference of two plane waves

Photoanisotropic polarization gratings are recorded by using a technique called *polarization holography*. The pattern to be recorded is formed by the interference of two plane waves with orthogonal polarization states. To introduce notations we briefly consider this interference pattern.

Consider two monochromatic plane waves (see Fig. 1) propagating in an (initially) isotropic medium with real refractive index n, having wave vectors in the $y = 0$ plane:

$$\mathbf{k}^{+} = (k_x, 0, k_z), \tag{1}$$

$$\mathbf{k}^{-} = (-k_x, 0, k_z), \tag{2}$$

#119008 - $15.00 USD Received 29 Oct 2009; revised 19 Dec 2009; accepted 22 Dec 2009; published 17 Mar 2010

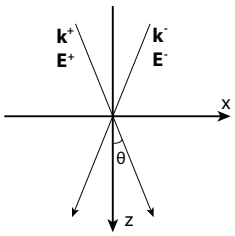

Fig. 1. Arrangement of the interference between two plane waves, with wave vector and complex fields $\mathbf{k}^+$, $\mathbf{E}^+$ and $\mathbf{k}^-$, $\mathbf{E}^-$ respectively.

where $k_z = (k_0^2 n^2 - k_x^2)^{1/2} > 0$ and $k_x > 0$ with k_0 the wave number in vacuum. From the figure, we see that $k_x = \sin\theta\, k_0$ and $k_z = \cos\theta\, k_0$. Without restricting generality, the electric vectors of the two plane waves are written in the form:

$$\mathbf{E}^+(\mathbf{r}) = \left[a_S^+ \begin{pmatrix} 0 \\ 1 \\ 0 \end{pmatrix} + a_P^+ \frac{1}{k_0 n} \begin{pmatrix} k_z \\ 0 \\ -k_x \end{pmatrix} \right] e^{i\mathbf{k}^+\cdot\mathbf{r}}, \tag{3}$$

$$\mathbf{E}^-(\mathbf{r}) = \left[a_S^- \begin{pmatrix} 0 \\ 1 \\ 0 \end{pmatrix} + a_P^- \frac{1}{k_0 n} \begin{pmatrix} k_z \\ 0 \\ k_x \end{pmatrix} \right] e^{i\mathbf{k}^-\cdot\mathbf{r}}, \tag{4}$$

where $a_S^\pm$ and $a_P^\pm$ are complex numbers. The electric field vector of each wave is thus decomposed into two orthogonal linear polarizations, namely the *s*- and *p*-polarization, where '*p*' means that the electric field is parallel to the (x,z)-plane, which is the plane through the wave vectors, and '*s*' means that the electric field is perpendicular to that plane. The '$+$' sign indicates that the x-component of the wave vector is positive, while the '$-$' sign has analogous meaning. The total electric field at $\mathbf{r}$ is the sum of the two separate fields of the plane waves:

$$\begin{aligned} \mathbf{E}(\mathbf{r}) &= \mathbf{E}^+(\mathbf{r}) + \mathbf{E}^-(\mathbf{r}) \\ &= \begin{pmatrix} (a_P^- e^{-ik_x x} + a_P^+ e^{ik_x x}) \frac{k_z}{k_0 n} \\ a_S^- e^{-ik_x x} + a_S^+ e^{ik_x x} \\ (a_P^- e^{-ik_x x} - a_P^+ e^{ik_x x}) \frac{k_x}{k_0 n} \end{pmatrix} e^{ik_z z}, \end{aligned} \tag{5}$$

and the physical total electric field is thus:

$$\mathscr{E}(\mathbf{r},t) = \mathrm{Re}\left[\mathbf{E}(\mathbf{r}) e^{-i\omega t}\right], \tag{6}$$

with $\omega > 0$. Note that this expression is for the most general situation, which is not limited to small recording angles or to certain polarization states.

We shall consider two cases in more details, namely the interference of two orthogonally circularly polarized beams and that of two orthogonally linearly polarized beams. Suppose first that the two incident waves are orthogonally circularly polarized with the same amplitude. Then in Eqs. (3), (4):

$$\left.\begin{aligned} a_S^- = a_S^+ = a_S, \\ a_P^- = -i a_S, a_P^+ = i a_S, \end{aligned}\right\} \tag{7}$$

with a_S real. Substitution into Eq. (5) gives for the total field of the two waves:

$$\mathbf{E}(\mathbf{r}) = 2a_S \begin{pmatrix} -\sin(k_x x) \frac{k_z}{k_0 n} \\ \cos(k_x x) \\ -i\cos(k_x x) \frac{k_x}{k_0 n} \end{pmatrix} e^{ik_z z}, \tag{8}$$

#119008 - $15.00 USD Received 29 Oct 2009; revised 19 Dec 2009; accepted 22 Dec 2009; published 17 Mar 2010

and

$$\mathscr{E}(\mathbf{r},t) = \mathrm{Re}\left[\begin{pmatrix} -2a_S \sin(k_x x)\frac{k_z}{k_0 n} \\ 2a_S \cos(k_x x) \\ -i2a_S \cos(k_x x)\frac{k_x}{k_0 n} \end{pmatrix} e^{i(k_z z-\omega t)}\right] = \begin{pmatrix} -2\frac{k_z}{k_0 n} a_S \sin(k_x x)\cos(k_z z-\omega t) \\ 2a_S \cos(k_x x)\cos(k_z z-\omega t) \\ 2\frac{k_x}{k_0 n} a_S \cos(k_x x)\sin(k_z z-\omega t) \end{pmatrix}. \quad (9)$$

The interference patterns for one modulation period P and for recording angles 2.5°, 10° and 15° are shown from top to bottom in Fig. 2. At the left, the polarization ellipses are shown for a number of equidistant points in one period. At the right, the intensity and the ellipticity are shown as function of position x.

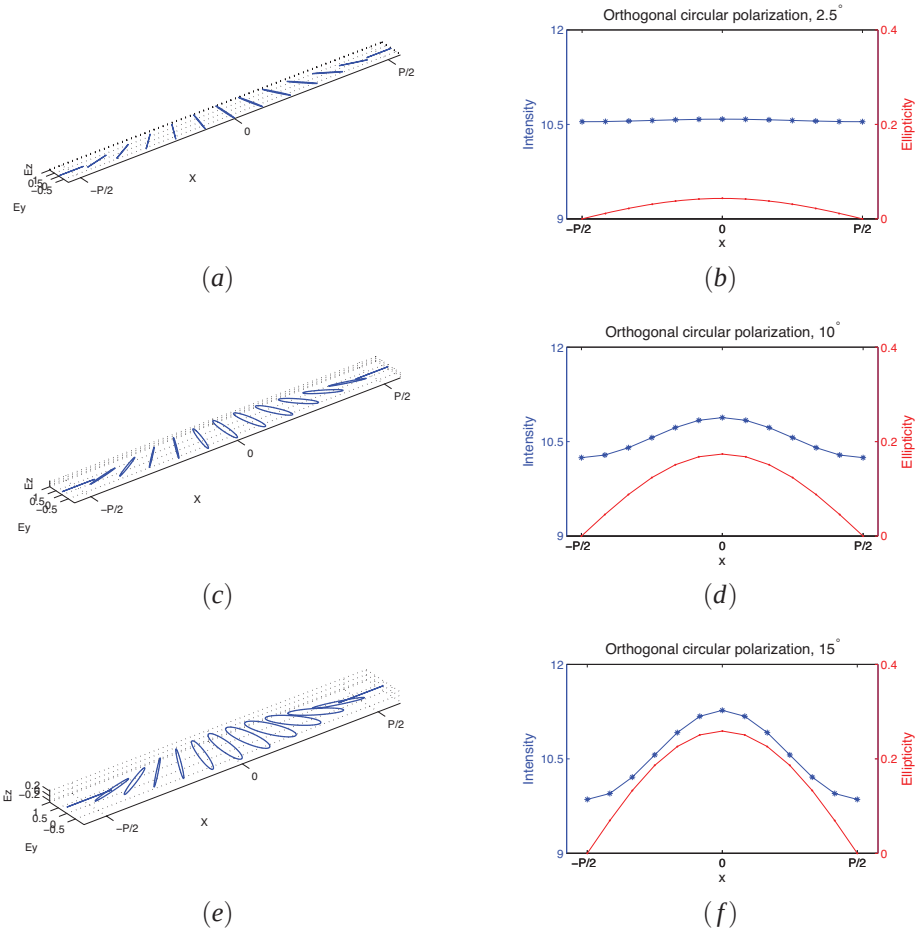

Fig. 2. (a) (c) (e) Polarization ellipses of the interference of two orthogonally circularly polarized plane waves with recording angle 2.5°, 10° and 15° respectively; (b) (d) (f) The ellipticity and total intensity modulation over one period of the pattern in (a), (c) and (e) respectively.

In the case of $\theta_{record.} = 2.5°$, the polarization state [see Fig. 2(a)] seems linear at each point over one modulation period. The ellipticity curve in Fig. 2(b) shows that in fact the field is elliptically polarized in most of the points, but that the ellipticity is small: $e < 0.05$, so that the polarization can consider to be linear everywhere. In this case, the intensity is almost constant.

#119008 - $15.00 USD Received 29 Oct 2009; revised 19 Dec 2009; accepted 22 Dec 2009; published 17 Mar 2010

Notice that in Fig. 2(b), 2(d), and 2(f) the scales are the same. Thus it is easy to see that when the angle of recording becomes bigger, the amplitude of the modulation in both intensity and polarization gets larger. It can also be seen from Figs. 2(c) and 2(e), that the polarization state is often elliptic. Furthermore, the plane of polarization rotates over 180° around the z-axis when x varies over one period. This complicates the description of the polarization states as will be seen below.

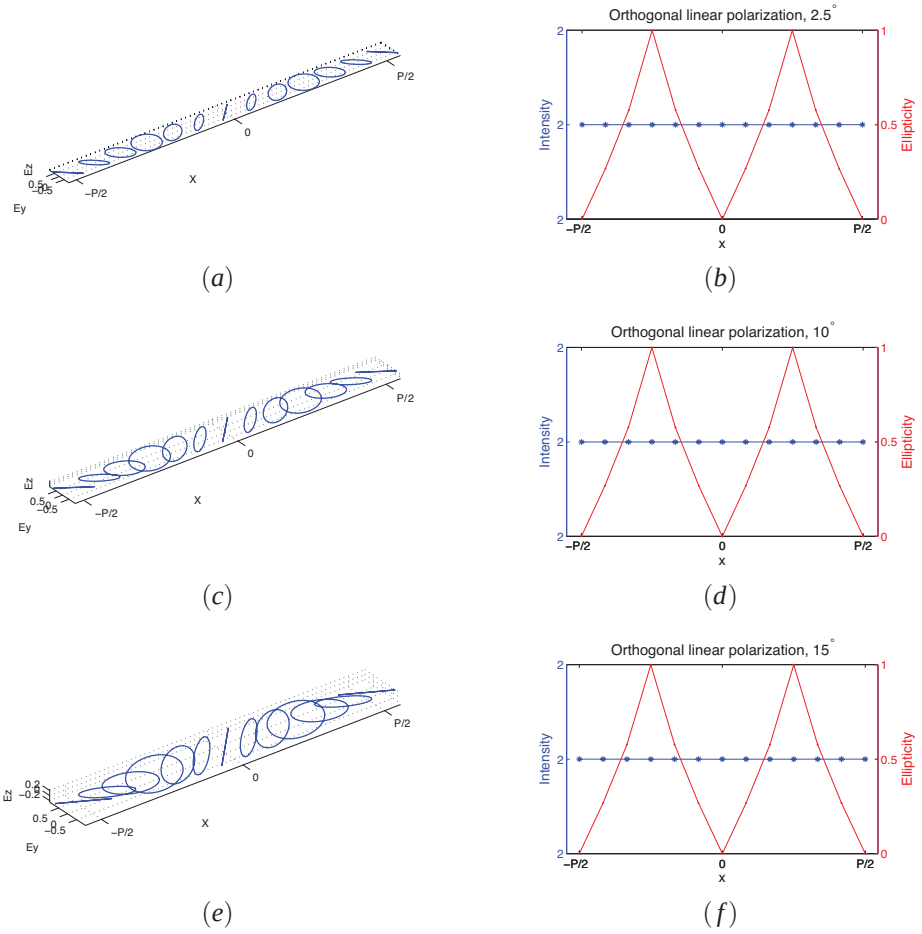

Fig. 3. (a) (c) (e) Polarization ellipses of the interference of two orthogonally linearly polarized plane waves with recording angle 2.5°, 10° and 15° respectively; (b) (d) (f) The ellipticity and total intensity modulation over one period of the pattern in (a), (c) and (e) respectively.

Next we consider the interference of two orthogonally linearly polarized beams. We assume that one is s- and the other is p-polarized with equal intensities:

$$\left.\begin{array}{ll} a_S^+ = a, & a_P^+ = 0; \\ a_S^- = 0, & a_P^- = a. \end{array}\right\} \tag{10}$$

#119008 - $15.00 USD Received 29 Oct 2009; revised 19 Dec 2009; accepted 22 Dec 2009; published 17 Mar 2010

The total field of the two waves is then

$$\mathbf{E}(\mathbf{r}) \quad = \quad a \begin{pmatrix} \frac{k_z}{k_0 n} e^{-ik_x x} \\ e^{ik_x x} \\ \frac{k_x}{k_0 n} e^{-ik_x x} \end{pmatrix} e^{ik_z z}. \tag{11}$$

The interference patterns for recording angles of 2.5°, 10° and 15° are shown in Fig. 3. It is seen that the intensity is constant in all cases. Furthermore, the state of polarization changes from linear to elliptic to circular and back to linear again (see the ellipticity curves in Fig. 3(b), 3(d), and 3(f). Figure 3(a), 3(c), and 3(e) show that for small recording angle the plane of polarization is almost identical to the (x,y)-plane, but that for larger recording angles the plane varies.

2.2. Representations of the states of polarization

In the most general form, the state of polarization of an arbitrary electric field is specified by 5 parameters:

- *two angles* to fix the direction of the unit normal of the polarization ellipse, chosen such that its direction corresponds to the sense of rotation of the electric field as a right handed screw drive.
- *a unit vector in the plane of the polarization ellipse* to specify the direction of the long axis of the ellipse;
- *ellipticity*;
- *intensity*.

Hence, to describe the modulation of the field over one period, we need to specify these five parameters as function of x. The conventional representation uses the *Poincaré sphere* [31]. This method describes the electric field in terms of only 3 parameters, which thus requires that two of the five parameters are constant for all states. As will be shown, for small angles between the wave vectors $\mathbf{k}^+$ and $\mathbf{k}^-$, the Poincaré sphere is adequate [27], but for larger angles this is not true.

2.2.1. Small recording angles

Suppose that the angle of recording is small, so that $k_x \approx 0$ and $k_z \approx k_0 n$. Then Eq. (5) becomes approximately:

$$\begin{aligned} \mathbf{E}(\mathbf{r}) \quad &= \quad \mathbf{E}^+(\mathbf{r}) + \mathbf{E}^-(\mathbf{r}) \\ &\approx \quad \begin{pmatrix} (a_P^- e^{-ik_x x} + a_P^+ e^{ik_x x}) \frac{k_z}{k_0 n} \\ a_S^- e^{-ik_x x} + a_S^+ e^{ik_x x} \\ 0 \end{pmatrix} e^{ik_z z}. \end{aligned} \tag{12}$$

The z-component vanishes then in good approximation, which means that the electric field is confined to the (x,y)-plane everywhere. The electric field can therefore be written as:

$$\mathbf{E}(x) = E_x(x)\hat{\mathbf{x}} + E_y(x)\hat{\mathbf{y}}. \tag{13}$$

Such a field can be represented by *Stokes parameters* and its state of polarization can be well represented on *Poincaré sphere*.

#119008 - $15.00 USD Received 29 Oct 2009; revised 19 Dec 2009; accepted 22 Dec 2009; published 17 Mar 2010

2.2.2. Large recording angles

In order to use the Poincaré sphere, all the polarization states have to be defined on the same basis in the common plane of polarization. When the recording angle is large, the Poincaré sphere is not applicable, since the plane of polarization rotates in 3D space due to the presence of the z-component of the electric field. In this case a local orthonormal basis $\{\hat{\mathbf{e}}_1(x), \hat{\mathbf{e}}_2(x), \hat{\mathbf{e}}_3(x)\}$ is defined such that $\hat{\mathbf{e}}_1(x)$ and $\hat{\mathbf{e}}_2(x)$ are along the long and short axes, respectively, of the polarization ellipse, and such that the electric field rotates in the direction from $\hat{\mathbf{e}}_1(x)$ to $\hat{\mathbf{e}}_2(x)$ and finally $\hat{\mathbf{e}}_3(x) = \hat{\mathbf{e}}_1(x) \times \hat{\mathbf{e}}_2(x)$. For a detailed derivation of the local basis, see Ref. [29]. This local basis is different for different points in space. Consider for example the interference of two elliptically polarized beams with:

$$\begin{aligned} a_S^+ &= 1, \quad & a_p^+ &= i; \\ a_S^- &= 1.5, \quad & a_P^- &= -2i, \end{aligned} \tag{14}$$

with recording angle 10°. The interference pattern formed by these two beams is shown at the

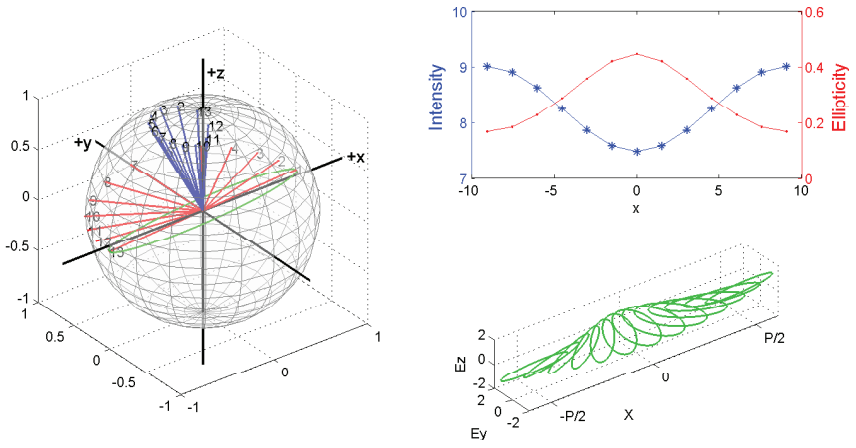

Fig. 4. Single-frame excerpt from Media 1 polarization representation of interference pattern of two elliptically polarized waves (Media 1).

right of Fig. 4 (Media 1). From the plot we can see that over one period, the states of polarization are elliptic everywhere. The ellipticity is shown in the figure on the upper right together with the intensity. Besides the ellipticity and the intensity, the other three parameters, namely, *two angles* to fix the direction of $\hat{\mathbf{e}}_3$ and *one angle* to fix the direction of $\hat{\mathbf{e}}_1$, are illustrated on the unit sphere shown in Fig. 4 on the left. For each state of polarization plotted at the right, the $\hat{\mathbf{e}}_1$, major axis of the polarization ellipse, is plotted as a unit vector in red color on the Cartesian basis, and $\hat{\mathbf{e}}_3$, which is normal to the plane of polarization, is plotted as a blue unit vector. All of the vectors are on the unit sphere.

The figures show clearly that the major axis of the polarization ellipse rotates 180° over one period of modulation, and that the plane of polarization also rotates. Thus the five parameters that determine the state of polarization of the vector field are all displayed in the left and upper right figures.

#119008 - $15.00 USD Received 29 Oct 2009; revised 19 Dec 2009; accepted 22 Dec 2009; published 17 Mar 2010

3. Characterization of the diffraction efficiencies of photoanisotropic polarization gratings with FEM

The recorded photo-anisotropy in the photoactive medium is described by an x-dependent relative permittivity tensor. This tensor is on the local basis $\{\hat{\mathbf{e}}_1(x), \hat{\mathbf{e}}_2(x), \hat{\mathbf{e}}_3(x)\}$ given by [17, 25]:

$$\underline{\underline{\tilde{\varepsilon}}}(x) = \begin{pmatrix} \varepsilon^i + \kappa_{\|}|E_1(x)|^2 + \kappa_{\perp}|E_2(x)|^2 & -i\kappa_c 2|E_1(x)||E_2(x)| & 0 \\ i\kappa_c 2|E_1(x)||E_2(x)| & \varepsilon^i + \kappa_{\perp}|E_1(x)|^2 + \kappa_{\|}|E_2(x)|^2 & 0 \\ 0 & 0 & \varepsilon^i + \kappa_{\perp}[|E_1(x)|^2 + |E_2(x)|^2] \end{pmatrix}, \tag{15}$$

where ε^i is the initial permittivity constant of the isotropic medium; $E_1(x)$ and $E_2(x)$ are the electric field components on the basis along the long and short semi-axes of the polarization ellipse respectively; and $\kappa_{\|}$, $\kappa_{\perp}$ and κ_c (in the unit of $\mathrm{m}^2/\mathrm{V}^2$) characterize the sensitivity of the photoanisotropic medium. The quantities $\kappa_{\|}$ and $\kappa_{\perp}$ are called the sensitivities of the linear photoanisotropy parallel and perpendicular to the principal molecular axis. The quantity κ_c is the sensitivity to circular photoanisotropy. The 'tilde' in $\underline{\underline{\tilde{\varepsilon}}}(x)$ is (and will be) used to emphasize that the relative permittivity tensor is written on the local basis $\{\hat{\mathbf{e}}_1(x), \hat{\mathbf{e}}_2(x), \hat{\mathbf{e}}_3(x)\}$. By applying a coordinate transformation, the permittivity tensor can be written on the global Cartesian basis $\{\hat{\mathbf{x}}, \hat{\mathbf{y}}, \hat{\mathbf{z}}\}$. Let

$$U(x) = (\hat{\mathbf{e}}_1(x), \hat{\mathbf{e}}_2(x), \hat{\mathbf{e}}_3(x)), \tag{16}$$

be the matrix with columns the unit vectors $\hat{\mathbf{e}}_j(x)$, $j = 1, 2, 3$. Then the permittivity matrix on the global basis $\{\hat{\mathbf{x}}, \hat{\mathbf{y}}, \hat{\mathbf{z}}\}$ is:

$$\underline{\underline{\varepsilon}}(x) = U(x)^* \underline{\underline{\tilde{\varepsilon}}}(x) U(x). \tag{17}$$

Note that when the material is an active medium, i.e. $\kappa_c \neq 0$ and the interference of the recording beams is not purely linear polarized everywhere ($S_3 \neq 0$), the permittivity tensor becomes complex hermitian. We remark here that the discussion and consideration are carried out under the assumption that the recording process is instantaneous and all the chemical and mechanical changes upon the irradiation of the light are immediate. The mechanism of the recording process is rather complicated and is beyond the scope of this paper.

To calculate the diffraction efficiency from such a grating rigorously, a numerical approach becomes necessary. We use the Finite Element Method (FEM) which is sufficiently general so that also position dependent Hermitian permittivity tensors can be simulated [32, 33].

We remark that the present model differs from the one described in [32, 33] regarding the numerical method that is used to solve the discretized linear system of equations. In [32, 33] an iterative method was used with approximate minimum fill-in reordering and a preconditioner from ILUPACK of Yousef Saad and Matthias Bollhoefer (see [34]). This preconditioning requires a lot of memory, in particular for three dimensional problems. In the present version of the code the sparse linear solver Pardiso [35, 36] is used. Due to this not only much less memory is needed, but also the computation time has been reduced drastically.

There is no strict limitation when the FEM code is applied. It can be used for periodic and non-periodic structure; 2D and 3D space; different materials including dielectric, metallic, isotropic, and anisotropic (hermitian permittivity tensor). When the material has nonlinear response, an iteration has to be made such that each time the program is called, a new permittivity tensor is put in the simulation as the material properties change with respect to time due to the nonlinear reaction. In such a way, the code can be applied to nonlinear materials as well.

3.1. OC polarization gratings

3.1.1. Angular dependence

Consider a grating recorded under the conditions: $\lambda_{record.} = 351$ nm, $\theta_{record.} = 2.5^\circ$, $\kappa_{\|} = 0.2\ \mathrm{m}^2/\mathrm{V}^2$, $\kappa_{\perp} = \kappa_c = 0$. Then the matrix $\underline{\underline{\tilde{\varepsilon}}}$ is diagonal and independent of x. Two of the diag-

#119008 - $15.00 USD Received 29 Oct 2009; revised 19 Dec 2009; accepted 22 Dec 2009; published 17 Mar 2010

onal elements are identical and therefore the medium is locally uniaxial with local optical axis along the $\hat{\mathbf{e}}_1(x)$ direction. The local ordinary and extraordinary refractive indices, $n_o = 1.5$ and $n_e = 1.6925$, are independent of position. Although $\underline{\underline{\tilde{\varepsilon}}}$ is independent of x, the local basis varies with x and hence $\underline{\underline{\varepsilon}}$ is also x-dependent. The pitch then is $\Lambda = 4023$ nm. The reading beam has wavelength of 633 nm and is a p-polarized plane wave. In all simulation we take the amplitude of the incident electric field to be 1 V/m. The values of κ specified are then in $\mathrm{m}^2/\mathrm{V}^2$. If the incident field amplitude is not unity, the values of κ have to be rescaled in proportion to the reciprocal square field amplitude to keep the permittivity tensor the same.

For a *p*-polarized perpendicular incident beam we show in Fig. 5 the efficiencies of the transmitted diffracted orders. It is seen that most of the transmitted light goes into three orders,

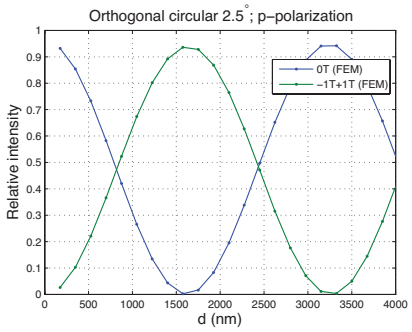

Fig. 5. Transmitted diffraction efficiencies as function of the grating thickness of an OC polarization grating recorded at $\theta_{record.} = 2.5^\circ$. The reading beam has wavelength 633 nm and is p-polarized. '-1T' in the legend represents the -1^{st} order in the transmitted field. Analogous conventions apply to 0T and 1T.

namely the 0^{th} and the $\pm 1^{st}$ orders. Polarization gratings are polarization selective. We observe that the polarization state of the 0^{th} order is always the same as that of the incident beam, while the polarization states of the two 1^{st} orders are always circular and orthogonal to each other. If the incident light is linear or unpolarized, both of the $\pm 1^{st}$ order propagate. When the incident polarization is circular, then depending on the handedness of the rotation, one of the first is absent. From Fig. 5, we see that when the grating has a thickness of 1575 nm, light is mostly diffracted into the first orders, with a small amount of light being reflected. Therefore we choose this optimized thickness for a 2.5° OC grating in the following discussion of the angular dependence.

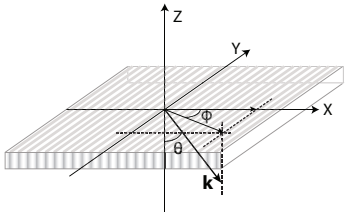

Fig. 6. The coordinate system and the definition of angles.

Let the plane of incidence first be the (x,z)-plane so that $\phi^i = 0^\circ$ (see Fig. 6 for the definition of the angles). The polar incident angle θ^i varies from 0° to 85°. For a 633 nm p-polarized incident field, the computed diffraction efficiencies for the transmitted and the reflected fields are shown in Fig. 7(a). In Fig. 7(b) the analogous results are shown for a *s*-polarized incident

#119008 - $15.00 USD Received 29 Oct 2009; revised 19 Dec 2009; accepted 22 Dec 2009; published 17 Mar 2010

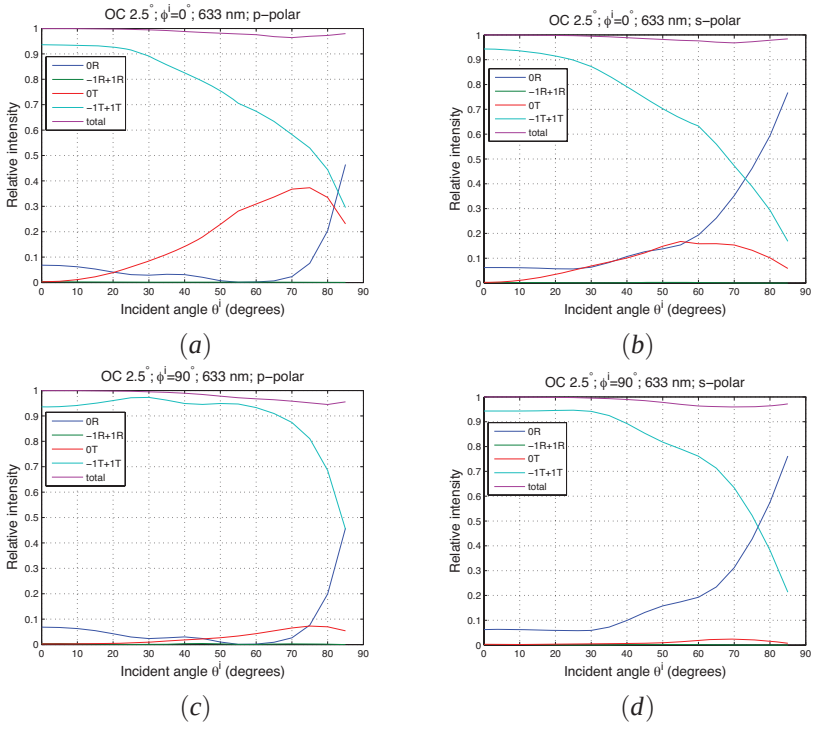

Fig. 7. Diffraction efficiency for OC polarization grating recorded at 2.5° as function of the incident angle. The reading beam is 633 nm, with (a) and (b) incident angles $\phi^i = 0°$ and (c) and (d) $\phi^i = 90°$. For both incidence mounts, θ^i varies from 0° to 85°. For (a) and (c), the incident wave is p-polarized and for (b) and (d), it is s-polarized.

wave. Comparing the two figures, we see that the diffraction efficiency is slightly different for the two linear polarizations. When θ^i increases, some light goes into the 2^{nd} orders in transmission which is not shown in the plots. When $\theta^i \leq 20°$, more than 90% of the incident light goes into the first orders. As θ^i rises to 40° the OC grating still gives rather high performance for both polarizations, where diffraction efficiency in the first orders is as high as 80%.

Next the plane of incidence is taken to be the (y,z)-plane, i.e. $\phi^i = 90°$. For varying θ^i, the diffraction efficiencies are again computed for both s- and p-polarization and the results are shown in Fig. 7(c) and 7(d), respectively. It is seen that the diffraction efficiency of the first orders for $\theta^i = 90°$ is higher than for $\theta^i = 0°$. For p-polarization, up to $\theta^i = 65°$, the intensity in the first order remains higher than 90%. For both polarizations the transmitted 0^{th} order is quite low compared to the previous case ($\phi^i = 0°$).

For both linear polarizations, at large θ^i, more light goes into the 0^{th} order in both transmission and reflection than for small θ^i. Furthermore, for *s*-polarized incident wave, the 0^{th} order reflection is for large θ^i larger than for the *p*-polarized incident wave. This can be understood using *Brewster* angle:

$$\theta_B = \arctan \frac{n_2}{n_1}, \tag{18}$$

by substituting $n_1 = 1$ and setting n_2 equal to the average refractive index of the polarization gratings, which is between 1.5 and 1.7. This gives an estimated range for the Brewster angle between 56° and 60°, which agrees with Fig. 7(a) and 7(c).

To summarize, when the angle of incidence θ^i is smaller than 30°, the diffraction from a OC

#119008 - $15.00 USD Received 29 Oct 2009; revised 19 Dec 2009; accepted 22 Dec 2009; published 17 Mar 2010

polarization grating is hardly sensitive to the angle of incidence. In this region, more than 90% light is diffracted into the 1^{st} orders. As θ^i gets larger, light gradually goes into the reflected and transmitted 0^{th} orders. At the same time, a small fraction of light leaks into the transmitted 2^{nd} orders. The insensitivity to the angle of incidence of the OC grating makes it suitable for applications that require large conical angle tolerance, such as in backlights for flat panel display systems.

3.1.2. Influence of the local linear birefringence

In the above case, the local linear birefringence $\Delta n = n_e - n_o$ is approximately 0.2. Material exhibiting such high birefringence is rare, except for LC. Therefore, we explore the influence of the local linear birefringence of the OC grating on its diffraction efficiencies.

Suppose that the grating has pitch of 4023 nm. The recorded local ordinary and extraordinary refractive indices are: $n_o = 1.5$ and $n_e = 1.6$. Thus the local linear birefringence is 0.1. For a perpendicular incident p-polarized plane wave with wavelength of 633 nm, the thickness dependence diffraction efficiency of the grating is shown in Fig. 8. It is shown clearly that the

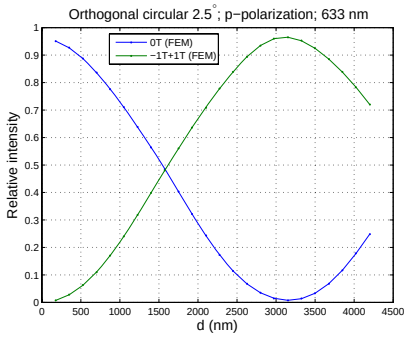

Fig. 8. Transmitted diffraction efficiencies as function of the grating thickness of an OC polarization grating with pitch of 4023 nm with local linear birefringence of 0.1. The reading beam has wavelength 633 nm and is p-polarized.

smaller local linear birefringence results in a much thicker grating to obtain the maximum first order transmission. With local linear birefringence of 0.1, the optimum thickness is 3150 nm, which is double of the previous case.

Analogously, the angular dependence of the grating is shown in Fig. 9. When $\phi^i = 0^\circ$, diffraction efficiency in the first orders for both s- and p-polarizations decline faster than that of the previous case with larger local linear birefringence. As contrast, when $\phi^i = 90^\circ$, the diffraction efficiencies with respect to the incident angle are almost the same as in the previous case and the influence of the reduction in the local birefringence is negligible. This can be further confirmed in the grating with even smaller local birefringence of 0.05.

For grating with local refractive indices: $n_o = 1.5$ and $n_e = 1.55$, the optimum thickness of the grating for the maximum first order transmission is 6300 nm which is observed with the FEM simulations. The figure is omitted here. The angular dependent diffraction efficiencies are shown in Fig. 10 for only p-polarization which should be effective to demonstrate the case. It is clear to see that, for such small local birefringence, the angular dependence of the diffraction efficiency is much stronger, and the high diffraction efficiencies in the first orders only exist for a small range of angles of incidence around the normal.

#119008 - $15.00 USD Received 29 Oct 2009; revised 19 Dec 2009; accepted 22 Dec 2009; published 17 Mar 2010

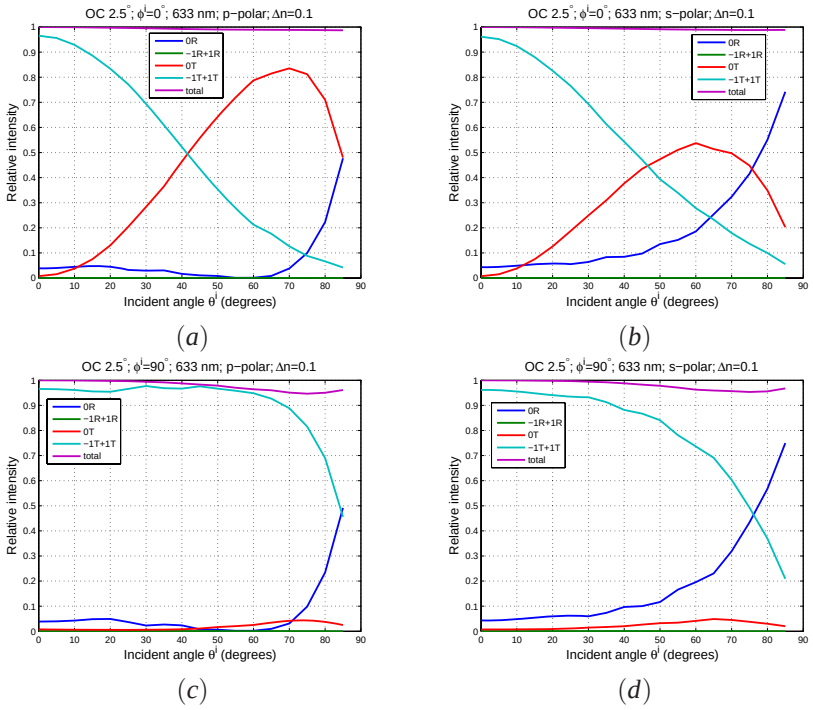

Fig. 9. Angular dependence diffraction efficiency for OC polarization grating with pitch of 4023 nm and with local linear birefringence of 0.1. The reading beam is 633 nm, with (a) and (b) incident angles $\phi^i = 0^\circ$ and (c) and (d) $\phi^i = 90^\circ$. For both incidence mounts, θ^i varies from 0° to 85°. For (a) and (c), the incident wave is p-polarized and for (b) and (d), it is s-polarized.

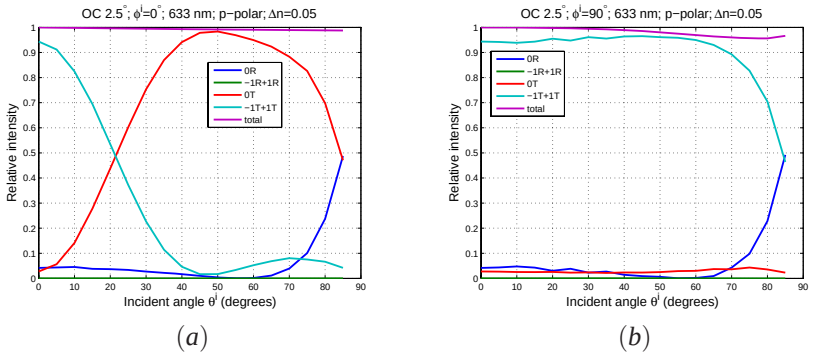

Fig. 10. Angular dependence diffraction efficiency for OC polarization grating with pitch of 4023 nm and with local linear birefringence of 0.05. The reading beam is 633 nm and p-polarized, and is incident at (a) $\phi^i = 0^\circ$ and (b) $\phi^i = 90^\circ$.

#119008 - $15.00 USD Received 29 Oct 2009; revised 19 Dec 2009; accepted 22 Dec 2009; published 17 Mar 2010

3.1.3. Beyond small recording angles

When larger recording angles are used, a grating with smaller pitch can be made. For a UV beam of 351 nm, the pitches obtained by using a number of recording angles are listed in Table 1.

Table 1. A few specific recording angles and the corresponding obtained pitches.

$\theta_{record.}$	Λ (nm)
2.5°	4023
10°	1011
15°	678

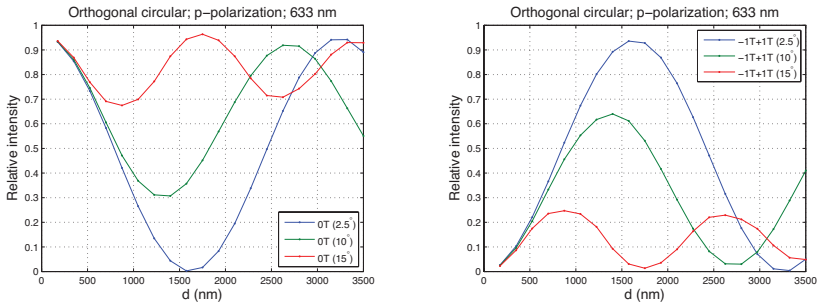

(a) (b)

Fig. 11. Comparison of the transmitted diffraction efficiency for a OC polarization gratings recorded at angles $\theta_{record.} = 2.5°$ (blue), 10° (green) and 15° (red). In (a) the diffraction efficiencies of the 0^{th} orders of the transmitted field, and in (b) shows the efficiencies of the transmitted 1^{st} orders are shown.

We consider OC polarization gratings recorded in a material with the photosensitivity as follows, $\kappa_{\parallel} = 0.2\ \mathrm{m}^2/\mathrm{V}^2, \kappa_{\perp} = \kappa_c = 0$. The reading light has a wavelength of 633 nm and is a p-polarized perpendicular incident plane wave ($\theta^i = 0°, \phi^i = 0°$). The efficiencies of the transmitted 0^{th} and 1^{st} orders are shown in Fig. 11 as function of the thickness of the grating for three recording angles, namely 2.5° (blue), 10° (green) and 15° (red). The curves for 2.5° are reproduced from Fig. 5 for comparison.

From Fig. 11, we can see that, although the shape of the curves are similar, for smaller pitch, the diffraction efficiencies of the 1^{st} orders drop considerably and more light goes into the 0^{th} transmitted order. At the optimum thickness for the diffraction efficiencies of the transmitted 1^{st} order is maximum, the 1^{st} order efficiency is for 10° 30% smaller and for 15° even 70% smaller than the maximum efficiency at 2.5°. This drop in diffraction efficiency is due to the increase of the ratio between the reading wavelength and the pitch of the grating. By using a shorter reading wavelength, the diffraction efficiency can be improved. In Fig. 12 the diffraction efficiencies of the grating recorded at 10° are shown for two reading beams at perpendicular incidence with wavelength of 532 nm and 450 nm. The results for a wavelength of 633 nm are reproduced for comparison. The pitch of this grating is approximately 1 μm (see Table 1). For smaller reading wavelengths (see Fig. 12), the diffraction efficiency of the 1^{st} orders is much higher. For 450 nm light, 90% light goes into the 1^{st} orders. It can be inferred from the figure that to optimize the performance of the grating for shorter wavelength, the grating has to be made thiner. When liquid crystals would be used, the manufacture would be challenging.

#119008 - $15.00 USD Received 29 Oct 2009; revised 19 Dec 2009; accepted 22 Dec 2009; published 17 Mar 2010

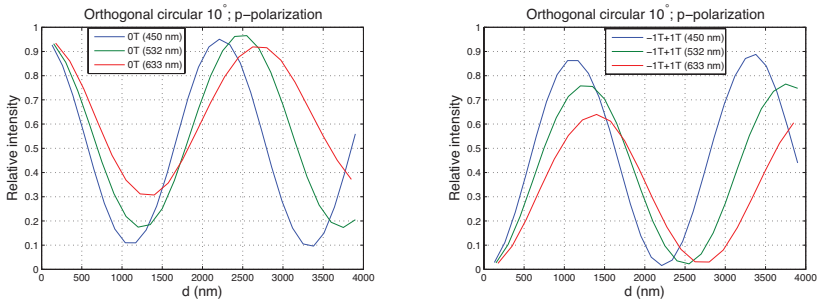

Fig. 12. Wavelength dependence of the diffraction efficiency of an OC polarization grating recorded at 10°. In the figure, blue, green, and red lines indicate 450 nm, 532 nm and 633 nm respectively. The incident wave is p-polarized and at perpendicular incidence, i.e. with $\theta^i = 0^\circ, \phi^i = 0^\circ$. Panel (a) shows relative intensity for the 0^{th} order in transmission and (b) for the 1^{st} transmitted orders.

3.2. OL polarization gratings

3.2.1. Thickness Dependence

For the OC gratings, we assumed that there is no circular anisotropy in the material, i.e. $\kappa_c = 0$. Therefore the dielectric permittivity was a real symmetric tensor of rank 2. This assumption was made because of the small ellipticity of the polarization states of the interference pattern of the two orthogonally circularly polarized beams. In the making of OL grating, two orthogonally linearly polarized beams are used. The states of polarization over one period of the interference in this case changes from linear through elliptic to circular and the ellipticity varies from 0 to 1. In this case, the modulation in ellipticity is significant. To record it, the material need to have circular photosensitivity, i.e. $\kappa_c \neq 0$. In previous work [29], we have shown that for small recording angles, and when $\kappa_c = \kappa_\parallel/2$, the obtained grating yields only three propagating transmitted orders, namely the 0^{th} and the $\pm 1^{st}$ orders. This specific case is considered as the *perfect* condition for OL gratings. For an OL grating, the dielectric permittivity is complex hermitian.

Suppose that the OL polarization grating is recorded under the following conditions: the polarization states of the recording beams are *s* and *p*; the two beams have equal amplitude; the recording angle is 2.5°. Let the photoanisotropy sensitivity of the material be $\kappa_\parallel = 0.2\ \mathrm{m}^2/\mathrm{V}^2$, $\kappa_\perp = 0$ and $\kappa_c = 0.1\ \mathrm{m}^2/\mathrm{V}^2$. The two real refractive indices on the basis of the eigenvectors are $n_1 = 1.6955$, $n_2 = 1.5$, assuming again that the amplitude of electric writing field is 1 V/m. To be clear, those parameters are not directly related to a real material. We comment here that circular photosensitivity is of higher order and can occur only in chiral materials. Here we calculated this ideal case to gain insight. The influence of the circular photosensitivity will be studied further in a later section.

For a perpendicular incident *s*-polarized reading beam with wavelength 633 nm, the diffraction efficiencies are shown as function of the thickness of the grating in Fig. 13. It is seen that only the 0^{th} and the -1^{st} orders propagate, while the $+1^{st}$ order is absent. This asymmetry is caused by the polarization selectivity of the polarization gratings, which we have discussed in [27]. When the incidence field is s-polarized, the transmitted first order is p-polarized, and vice versa. In contrast, the polarization of the 0^{th} order is always the same as that of the incidence. If the incident beam is circular polarized, the transmitted field has three propagating orders, namely the 0^{th} order with the same circular polarization as the incidence and the $\pm 1^{st}$

#119008 - $15.00 USD Received 29 Oct 2009; revised 19 Dec 2009; accepted 22 Dec 2009; published 17 Mar 2010

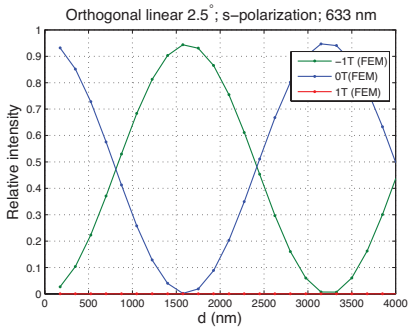

Fig. 13. Diffraction efficiency of an OL polarization grating recorded at $\theta_{record.} = 2.5^\circ$ as function of the thickness of the grating. The reading beam has wavelength of 633 nm and is an s-polarized perpendicular incident plane wave. '-1T' in the legend represents the -1^{st} order in the transmitted field. Analogous conventions apply to 0T and 1T.

orders with orthogonal linear polarization states.

At the thickness of 1575 nm, the efficiency of the transmitted 1^{st} order is maximum and that of the 0^{th} order vanishes. We will consider this thickness in the following study of the diffraction at oblique incidence.

3.2.2. Angular dependence

Analogous to the plots in Section 3.1.1 the simulations for OL at oblique incidence are performed for both *s*- and *p*-polarized reading beams. The results are shown in Fig. 14. The total intensity of the plotted orders is almost equal to 1 for the entire range of incident angles. At large incident angles, the 2^{nd} transmitted order increases. The intensities of the reflected 1^{st} orders vanish, which means that the reflected light only excited the 0^{th} order. The insensitivity to angle of incidence for $\theta^i \leq 30^\circ$ is observed.

For plane of incidence of which $\phi^i = 0^\circ$, the polarization state of the reading beam is switched from *p* to *s* from Fig. 14(a) to Fig. 14(b). It is seen that an OL polarization grating acts as a linear polarization converter, and depending on the direction of the incident linear polarization state, only one of the $\pm 1^{st}$ transmitted orders propagates.

For plane of incidence such that $\phi^i = 90^\circ$, and for an s-polarized incident beam the $+1^{st}$ order is present instead of the -1^{st} as when $\phi^i = 0^\circ$. This can be explained by examining the electric vector of the reading beam. For $\phi^i = 0^\circ$, the electric field vector of *s*-polarization has components $E_x = 0, E_y = 1, E_z = 0$, hence the incident electric field is parallel to the *y*-axis. When $\phi^i = 90^\circ$, however, the electric field vector of *s*-polarization is then rotated over 90°. The same argument applies to *p*-polarization.

3.2.3. Beyond small recording angles

OL polarization gratings recorded at large angles 10° and 15° are studied. For a perpendicularly incident *s*-polarized plane wave, of 633 nm the efficiencies of the transmitted diffracted order are shown in Fig. 15 as function of the thickness. The small angle case of 2.5° is reproduced for comparison. It is clear from the figures, that larger recording angles lead to lower diffraction efficiencies. This result is similar to what we observed for OC polarization gratings in Section 3.1.3. Analogous to that case, the diffraction efficiency can be improved by using reading beam with shorter wavelength.

#119008 - $15.00 USD Received 29 Oct 2009; revised 19 Dec 2009; accepted 22 Dec 2009; published 17 Mar 2010

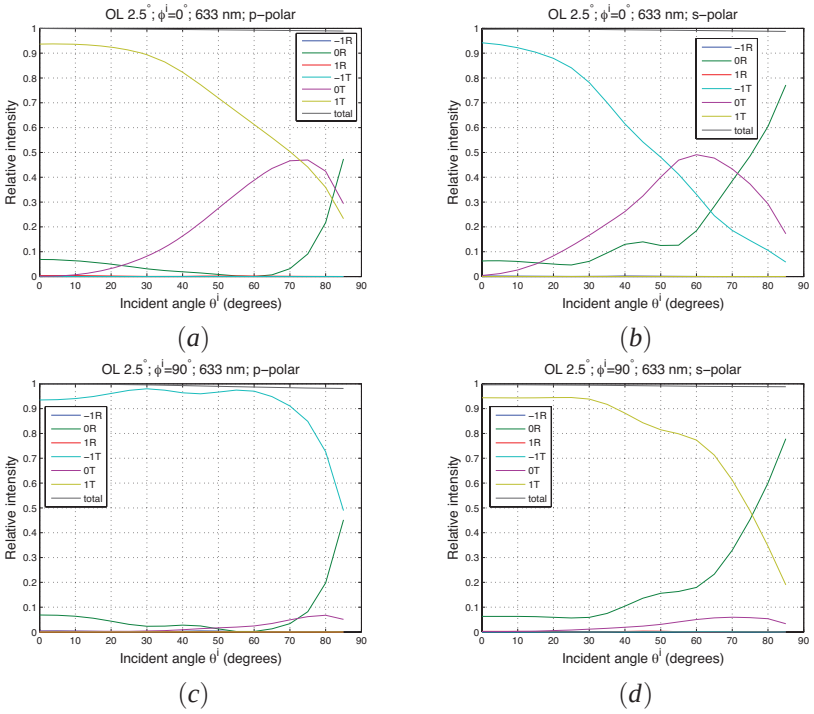

Fig. 14. Diffraction efficiency of an OL polarization grating recorded at 2.5° as function of the incident angle. The reading beam is 633 nm, with (a) and (b) incident angles $\phi^i = 0°$ and (c) and (d) $\phi^i = 90°$. For both incidence mounts, θ^i varies from 0° to 85°. For (a) and (c), the incident wave is p-polarized and for (b) and (d), it is s-polarized. -1T in the legend represents the -1^{st} order in the transmitted field. Analogous conventions apply to 0T and 1T. R represents the reflected field.

3.2.4. Imperfect OL polarization gratings – influence of κ_c

A critical requirement for a *perfect* OL polarization grating is that the photoanisotropic material must be sensitive to circular polarization ($\kappa_c \neq 0$) *and* that the circular anisotropy sensitivity κ_c must be half the linear anisotropy sensitivity $\kappa_c = \frac{\kappa_\parallel + \kappa_\perp}{2}$. However, circular photosensitivity is of higher order and is often much smaller than the linear photosensitivity of the material. The 'perfect' recording condition is rather difficult to fulfill. Therefore the influence of the circular photosensitivity of the material on the diffraction efficiencies of the grating is studied. For this case, we only consider OL gratings recorded at small recording angle 2.5° .

First, suppose that the recording medium is not active, i.e. $\kappa_c = 0$. All the other parameters are kept the same as in the thickness dependence study. As function of the thickness of the grating, the efficiencies of each propagating order is plotted in Fig. 16. Because many orders propagate in the transmitted field, we plot the total intensity of the transmitted field and the 0^{th} order in Fig. 16(a), and the other higher diffracted orders in Fig. 16(b). The total intensity is not 1, because a small amount of light is reflected into the 0^{th} order. In the transmitted field, there are nine nonzero propagating orders. When the grating is thicker, more diffracted orders emerge out of the grating in transmission. Instead of having only the -1^{st} order as in the 'perfect' case, now the $\pm 1^{st}$ orders have almost equal intensity. Furthermore, for every pair of $\pm 2^{nd}$, $\pm 3^{ed}$ and even $\pm 4^{th}$ orders, light is almost equally distributed. The polarization states of all orders are elliptical.

#119008 - $15.00 USD Received 29 Oct 2009; revised 19 Dec 2009; accepted 22 Dec 2009; published 17 Mar 2010

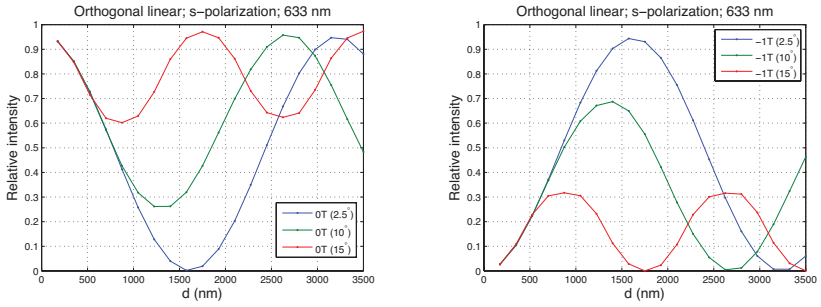

(a) (b)

Fig. 15. Comparison of diffraction efficiency of OL polarization gratings recorded at angles $\theta_{record.} = 2.5^\circ$ (blue), 10° (green) and 15° (red). Subfigure (a) shows the diffraction efficiency of the 0^{th} transmitted order, and subfigure (b) shows the efficiency of the transmitted 1^{st} orders.

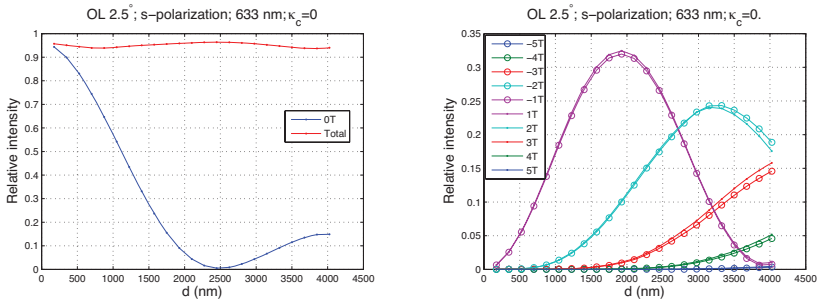

(a) (b)

Fig. 16. OL polarization grating with $\kappa_c = 0$. Panel (a) displays the relative intensity for 0^{th} order and total intensity in transmission; (b) displays higher diffracted orders in transmission.

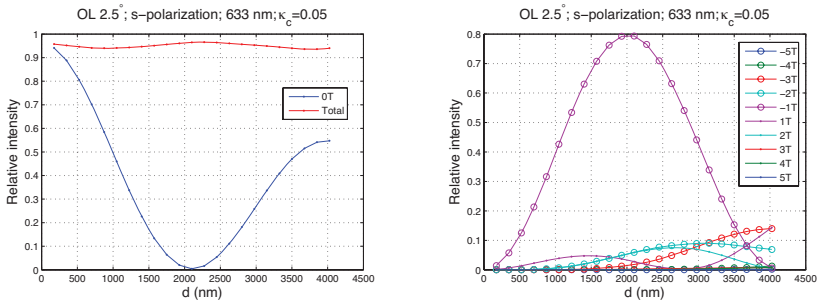

(a) (b)

Fig. 17. OL polarization grating with $\kappa_c = 0.05$. Panel (a) displays the relative intensity for the 0^{th} order and total intensity in transmission; (b) displays higher diffracted orders in transmission.

#119008 - $15.00 USD Received 29 Oct 2009; revised 19 Dec 2009; accepted 22 Dec 2009; published 17 Mar 2010

Next suppose that the medium has weak circular sensitivity: $\kappa_c = 0.05\ \mathrm{m}^2/\mathrm{V}^2$ (which is half of the optimum value). The results in Fig. 17 show that the diffraction efficiencies are in between those for the perfect OL grating and the one with $\kappa_c = 0$. For $\kappa_c = 0.05\ \mathrm{m}^2/\mathrm{V}^2$ the -1^{st} transmitted order dominates the transmitted field with a maximum efficiency of 80%. The thickness of the grating for which the diffraction of the -1^{st} order is maximum is 2000 nm. This is thicker than for the 'perfect' case (1575 nm).

We then conclude that the performance of the OL polarization grating is very sensitive to the value of κ_c. A small variation of it affects both the diffraction efficiency and optimal thickness of the grating. In practice, this complicates the manufacture of an OL grating considerably.

4. Conclusions

In this paper, we studied the photoanisotropic polarization gratings using rigorous diffraction calculation. We explained first that when the recording angle between the two beams is large, the conventional Poincaré sphere is not suitable to describe all polarization states that occur over a period. In fact, when the recording angle between the two recording beams is large, the interference pattern of two orthogonally polarized beams consists of periodic modulations of polarization states and intensity with the electric field not remaining in one plane. The plane of the polarization ellipse of the interference pattern rotates in 3D space. By introducing a local coordinate basis such that two of the basis vectors span the local plane to which the polarization ellipse is parallel, we described the modulation of the electric field using five parameters.

The diffraction efficiencies of both OC and OL polarization gratings are characterized by simulations. The results show that with polarization gratings very high diffraction efficiencies can be achieved, higher than 95% for appropriate thicknesses for only three diffraction orders in the transmitted field, namely the $\pm 1^{st}$ and 0^{th} orders. The dependence of the diffraction efficiencies on the incident angle of the reading beam is rather weak. For materials with relative large photosensitivity, within a range of 20° of incident angles, the diffraction efficiencies remain higher than 90% for both OC and OL polarization gratings. For OC grating with smaller local linear birefringence, the diffraction efficiencies have a much stronger dependence on the angle of incidence. Larger recording angles result in smaller pitches at the cost of lower diffraction efficiencies for the same wavelength of the reading beam. For OL polarization gratings, it is found that the value of the circular polarization sensitivity of the recording material is critical for a high diffraction efficiency.

Acknowledgments

This research has been done in TU Delft and is part of STW - Dutch Technology Foundation project DOE. 6823.

#119008 - $15.00 USD Received 29 Oct 2009; revised 19 Dec 2009; accepted 22 Dec 2009; published 17 Mar 2010